Energy Conversion and Management 245 (2021) 114337

Contents lists available at ScienceDirect

Energy Conversion and Management

journal homepage: www.elsevier.com/locate/enconman

An investigation of recovering the energy of exhaust heat for improving conventional compression ignition to low temperature combustion by adding diesel vapor

Mohsen Bashi, Mohsen Ghazikhani *

Dept. of Mechanical Engineering, Ferdowsi University of Mashhad, Azadi square, 9177948974 Mashhad, Iran

ARTICLE INFO

Keywords:
Exergy Analysis
Low Temperature Combustion
Chemical Exergy
Exhaust Heat Recovery

ABSTRACT

Reducing exhaust emissions and, consequently, recovering wasted energy and exergy of an engine are the primary purposes of engine research. In previous studies, improving the combustion efficiency and reducing the exhaust emissions by homogeneous combustion, and the recovery of engine wasted energy (especially exhaust wasted energy) to use in the downstream cycles have been researched. In the present study, the feasibility of recovering exhaust energy to evaporate diesel fuel and the effects of adding diesel vapor on combustion efficiency, exhaust emissions, and overall engine efficiency have been investigated. To achieve these purposes, an experimental investigation on the effects of adding diesel vapor was performed. And, the numerical analysis was used to investigate the feasibility of the diesel evaporation by recovering exhaust energy. The experimental tests were performed at a constant speed (1000 rpm) and three amounts of fuel injection. In each amount of fuel injection, the amount of diesel vapor increased in three steps up to the knock threshold. In the experimental investigation, the share of the indicated work, combustion irreversibilities, heat transfer loss, and exhaust gas from the inlet exergy have been shown. Also, the effects of adding diesel vapor on exhaust emissions (PM, NO, CO and HC) and the cycle variation were investigated. Furthermore, the chemical exergy of each one of the species in the exhaust stream was investigated in detail. In the numerical investigation, the following results were investigated: the available exhaust gas exergy up to the dew point, the share of the exhaust recoverable energy from the diesel evaporation energy, the improvement of the second law efficiency by recovering exhaust gas energy, the reduction of exhaust gas temperature, and the required length of heat exchanger for increasing the diesel temperature from ambient temperature up to the exhaust gas temperature. According to the achieved results, adding diesel vapor reduces combustion irreversibility and heat transfer loss; also, the second law efficiency improves from 30% to 44%. Using a heat exchanger can recover 20–45% of the required evaporation heat of diesel. The reduction of exhaust gas temperature after the heat exchanger is less than 2%. The maximum required heat exchanger length for increasing the diesel temperature from ambient temperature up to the exhaust gas temperature is 50 cm. The addition of diesel vapor decreases NO and soot emissions and, simultaneously, increases CO and HC emissions. The addition of diesel vapor decreases the cycle variation, especially in low-load conditions. According to the chemical exergy of the various species in the exhaust gas mixture, the CO2 and H2O emissions have the most destructive effect on the environment; also, the detrimental environmental impact of CO emission is more than NO until being oxidated by a catalyst.

1. Introduction

Internal combustion engines are, somehow, the smallest units of generating power from the chemical energy of the fuel. Despite short-run plans to remove these small power generators from cars, there is evidence of a lack of community support and financial resources spent on developing and feeding this equipment. Also, using internal combustion engines in ships, CHPs (Combined Heat and Power), and power plants means there is no alternative to them in the near future. In addition to this fact, according to the International Energy Agency report, the consumption of fossil fuels has increased annually without any decrease [1], and the share of transportation in CO2 emissions is not negligible [2]. The effects of air pollution have gone so far that, based on

* Corresponding author.
E-mail addresses: mohsenbashi@mail.um.ac.ir (M. Bashi), ghazikhani@um.ac.ir (M. Ghazikhani).

https://doi.org/10.1016/j.enconman.2021.114337
Received 13 March 2021; Accepted 24 May 2021

Nomenclature

$a_1 \cdots a_7$, b_1, b_2	NASA equations constants
c_P	Specific heat capacity at constant pressure
C_P	Heat capacity at constant pressure
COV	Coefficient Of Variation
D	Diameter
f	Friction factor
g_f	Specific gibbs energy of formation
h°	Standard specific enthalpy
h	Actual specific enthalpy
h_f	Specific enthalpy of formation
$h_{Conv.}$	Convective heat transfer coefficient
H	Actual enthalpy
HRR	Heat Release Rate
HE	Heat Exchanger
I	Irreversibility
$IMEP$	Indicated Mean Effective Pressure
k	Conductivity
K	Interaction conductivity
L	Length
$\dot{m}$	Mass flow rate
M_W	Molecular mass
M	Interaction viscosity
MFB	Mass Fraction Burn
$\dot{n}$	Molar flow rate
n	Cycle number
Nu	Nusselt number (local)
$Nu_{Developed}$	Fully developed Nusselt number
P	Pressure
Pr	Prandtl number
Q	Heat
$\widetilde{R}$	Universal gas constant
Re	Reynolds number
Rec.	Recovered
Req.	Required
s°	Standard specific entropy
s	Actual specific entropy
S	Actual entropy
T	Temperature
VP	Vapor Percent
$V_{Displacement}$	Displacement Volume
W_{Net}	Indicated Work
X	Exhaust wet mole fraction
x	Ambient air wet mole fraction
Y	Exhaust Dry mole fraction
y	Ambient air dry mole fraction
z	Enterance length
ε	Surface roughness
η_{II}	Second law efficiency, Effectivness
ρ	Density
μ	Viscosity
θ	Crank Angle
ψ	Specific stream exergy
Ψ	Stream exergy

Subcripts:

i	Species i
j	The step j in integral
Th.Ph.	Thermophysical
Chem	Chemical
–	Average
Mix	Mixture
0	Ambient Condition

the evidence found by Setti et al. in Italy [3], COVID-19 RNA (Ribo-Nucleic Acid) has been found on particulate matter (PM), which may be a sign of the severity of the disease in the areas surveyed by them. Other studies on the relationship among air pollutants effects (especially particulate matter and nitrogen oxides) on mortality rates in the COVID-19 pandemic have been conducted [4,5]. Therefore, research is ongoing to reduce the emissions of internal combustion engines and increase their efficiency. The proposed solutions for increasing efficiency and reducing emissions are the homogeneous combustion models and the recovering wasted energy.

In internal combustion engines, there are three main factors: incomplete air–fuel mixing, increasing local temperature, and flame front, which reduce efficiency and increase the formation of pollutants in the combustion process. In other words, homogeneous (complete mixing of fuel and air), spontaneous (without flame front), and dilute (with low combustion temperature) combustion increases efficiency and reduces engine emissions. This idea has led to various homogeneous combustion models such as HCCI (Homogeneous charge compression ignition), PCCI (Premixed Charge Compression Ignition), and RCCI (Reactivity Controlled Compression Ignition). Onishi in 1979 introduced HCCI engines [6], Aoyama in 1996 [7] and Kokjohn and Reitz in 2011 [8] coined the terms PCCI and RCCI, respectively. The reasons for the lack of success of homogeneous combustion models are the inability to operate in the full range of load and speed, the tendency to knock, the challenge of cold start, and the increasing carbon monoxide and unburnt hydrocarbons emissions. Duan et al. investigated the combustion control methods of HCCI engines [9]. According to the results of their study, since HCCI engines are highly dependent on the air–fuel composition characteristics, the combustion control methods correlate with controlling fuel quality, fuel (or fuels) reactivity, air–fuel stratification temperature, recirculated gas properties, and residual gas properties. Besides controlling air–fuel characteristics, one of the physical solutions for combustion control is using a spark plug. Shim et al. compared HCCI and PCCI engines in single-fuel mode and PCCI in dual-fuel mode to find an alternative to the CDC (Conventional Diesel Combustion) [10]. Based on their study results, all three studied combustion technologies can reduce NOx and PM below the Euro 6 standard level without exhaust gas aftertreatment. But controlling combustion of HCCI and single-fuel PCCI requires the use of more than 40% EGR (Exhaust Gas Recirculation) and multiple injections. The dual-fuel PCCI combustion is controlled easier by adjusting the amount of secondary fuel and the timing of diesel fuel injection. The three combustion models increase the emission of CO and HC (HydroCarbon). However, that is more significant in HCCI and single-fuel PCCI combustion. Singh et al. compared PCCI and RCCI combustion with conventional diesel [11]. According to their results, the PCCI engine has more tendency to knock than RCCI and conventional diesel engines. Also, the conventional diesel engine's thermal efficiency at low loads is higher than PCCI and RCCI engines. They concluded that RCCI combustion is more capable of balancing efficiency, emissions, load range, and speed range than PCCI and conventional diesel combustion. In a comprehensive review of the RCCI engine, Paykani et al. found that the use of alcohol (E85) instead of gasoline was influential in expanding the load range in transition conditions [12].

Besides the study and research on completely-homogeneous combustion, commercial vehicles have achieved good efficiency and performance by multiple fuel injection and semi-premixed combustion. Increasing the spray pressure reduces the diameter of the fuel droplets and mixes them better and faster with air, according to a literature review by Mohan et al. [13]. Better and faster mixing increases the pressure growth rate and reduces the ignition delay. As a result, NOx

(Nitrogen Oxides) production and the tendency to knock increase. Therefore, if the injection amount is reduced, the rapid growth of pressure and the increase of NOx production can be prevented. The multiple injections idea is based on forming a dilute homogeneous mixture to reduce NOx emission while increasing efficiency. The concept of adding fuel vapor is similar to multiple injections, thereby reducing the combustion temperature and NOx emission. Bharathiraja et al. [14] investigated on adding gasoline vapor to the inlet air of an engine. Sahin et al. [15] investigated on adding ethanol vapor to the inlet air of an engine. Both of them obtained similar results in reducing NOx emission and increasing efficiency. The idea under consideration in this paper (adding diesel vapor) is presented based on this regard. But unlike light fuels such as gasoline and ethanol, diesel fuel does not readily evaporate, and also, due to its heavy hydrocarbons, it can increase soot emission. With these advantages, there is no need for a secondary fuel tank in this proposal, and it is possible to evaporate diesel by using exhaust heat loss and injecting it into the inlet without installing a secondary injector.

In a compression ignition engine, 34–38% of the fuel energy is converted to work, 23–37% of the fuel energy is wasted through the exhaust gas, and 16–35% of it is wasted through the cooling system [16]. Thus, about two-thirds of the fuel energy in a typical diesel engine is wasted through the exhaust gas and cooling system. Due to the higher temperature of the exhaust gas versus the cooling system, the exhaust gas has higher availability than the cooling water. One of the most common ways to increase overall engine efficiency is the exhaust gas energy recovering methods, which are classified into two categories: direct and indirect. The common direct method is the turbocharger. Indirect methods mainly use the exhaust gas energy to drive downstream Rankine cycles or generators of absorption refrigeration systems. The low evaporation temperature of the working fluid of the Organic Rankine Cycles (ORC) and the absorption refrigeration cycles make these cycles ideal for exhaust heat recovery. However, studies have been performed on the Stirling and Kalina cycles [17]. The most important limitation of using downstream cycles is their cost, and their pieces of equipment include heat exchangers, turbines, and generators. Therefore, their main application is in the large heavy engines (especially in ships), which have enough space to install their equipment, and the large volume of exhaust gas causes significant energy losses [18–20]. Studies have been done on the installation of ORC on diesel engines of urban trucks [21]. Ravi and Pachamuthu placed a finned heat exchanger, covered with oxidation catalysts, in the path of the exhaust gas. According to their results, up to 17% of unburned hydrocarbons and 7% of nitrogen oxides were reduced [22]. Also, using an ORC cycle adds 7.6% of the fuel energy to the braking power, and the braking efficiency increased from 32% to 39.2% [23].

The present study consists of two parts: experimental and numerical. The numerical analysis was used to calculate the heat transfer from the exhaust gas to diesel in a heat exchanger. And, the experimental analysis was used to investigate the effects of adding diesel vapor on emissions and performance.

Table 1
The molar fraction of various species in atmospheric air [34].

Species	Dry Molar Fraction	Wet Molar Fraction x_i
N2	0.7808	$0.7808(1-x_{H_2O})$
O2	0.2095	$0.2095(1-x_{H_2O})$
H2O	–	$x_{H_2O}=\phi P_g(T_0)/P_0$
CO2	0.000345	$0.000345(1-x_{H_2O})$
Ar	0.009355	$0.009355(1-x_{H_2O})$

2. Equations and calculations

2.1. Exergy analysis

2.1.1. Molar flow of species in a mixture

For exergy analysis, it is necessary to calculate exhaust products' mole fraction by using gas analyzer recorded values. In the used analyzer, the output products passes through a filter, and its water vapor distills before entering the analyzer [24]. So, if the molar fraction measured by the analyzer is Y_i (dry basis), the molar fraction of that species in the engine output mixture is $X_i = Y_i(1 - X_{H_2O} - X_{Soot})$. The smoke meter input sample does not pass through a filter or water distiller; thus, the measured soot fraction is X_{Soot}. According to the "Smoke value measurement with the filter paper method", the soot fraction represents the carbon fraction [25]. The atmosphere compositions are shown in Table 1, and the Diesel surrogate was assumed Jet-A ($C_{12}H_{23}$); based on these assumptions, the combustion reaction for one mole of products is shown in Eq. (1). Diesel fuel is a composition of different hydrocarbons with different structures and different molecular mass. Many attempts have been done to introduce the surrogate fuel for diesel in chemical kinetic calculations. The diesel surrogate should be introduced in a way that correctly predicts exhaust emissions formation and especially soot formation in chemical kinetic calculation. n-Heptane (n means Normal) is one of the single component surrogate fuels, due to the same cetane number as diesel fuel [26]. Also, n-Dodecane is a single component surrogate fuel for diesel, because its carbon number (12) is in the diesel range (10–22) [27]. Due to the weakness of the single component diesel surrogates, the binary component diesel surrogate like n-Heptane/n-Butanol [28], n-Heptane/Toluene [29], n-Dodecane/m-Xylene [30], etc was studied and introduced. The surrogate fuels are introduced along with a chemical reaction mechanism that is used in chemical kinetic calculation. In the present study, no chemical kinetic calculation will be done, but the enthalpy and entropy of fuel in arbitrary temperature and pressure should be calculated. Therefore, in the absence of NASA (National Aeronautics and Space Administration) equation constants for diesel fuel, the NASA constants for another commercial fuel (Jet-A) whose carbon number is in the diesel range were used; instead of conventional diesel surrogates (n-Heptane, n-Dodecane, n-Dodecane/m-Xylene, …). Jet fuel is a commercial fuel and is useable in diesel engines [32,33].

$$X_{Fuel}C_{12}H_{23} + X_{Air}\left(O_2 + \frac{x_{N_2}}{x_{O_2}}N_2 + \frac{x_{H_2O}}{x_{O_2}}H_2O + \frac{x_{CO_2}}{x_{O_2}}CO_2 + \frac{x_{Ar}}{x_{O_2}}Ar\right) \rightarrow X_{H_2O}H_2O + X_{CO_2}CO_2 + X_{CO}CO + X_{NO}NO + X_{HC}C_3H_8 + X_{Soot}C + X_{O_2}O_2 + X_{N_2}N_2 + X_{Ar}Ar \quad (1)$$

The Eq. (2) simultaneous Equations are written based on the mass balance of Carbon, Hydrogen, and Oxygen atoms in Eq. (1) reaction. By solving these equations, the X_{Fuel}, X_{Air}, and X_{H_2O} were computed. To calculate $X_{N_2} = Y_{N_2}(1 - X_{H_2O} - X_{Soot})$, the equations

$Y_{O_2}+Y_{N_2}+Y_{CO_2}+Y_{CO}+Y_{HC}+Y_{NO}+Y_{Ar}=1$ and $Y_{Ar}=X_{Air}\frac{x_{Ar}}{x_{O_2}}/(1-X_{H_2O}-X_{Soot})$ were used.

$$\begin{cases} Carbon: \ 12X_{Fuel}+X_{Air}\dfrac{x_{CO_2}}{x_{O_2}}=X_{CO_2}+X_{CO}+3X_{HC}+X_{Soot} \\ Hydrogen: 23X_{Fuel}+2X_{Air}\dfrac{x_{H_2O}}{x_{O_2}}=2X_{H_2O}+8X_{HC} \\ Oxygen: X_{Air}\left(2+\dfrac{x_{H_2O}}{x_{O_2}}+2\dfrac{x_{CO_2}}{x_{O_2}}\right)=X_{H_2O}+2X_{CO_2}+X_{CO}+X_{NO}+2X_{O_2} \end{cases} \quad (2)$$

The various species mole fraction of a mixture (output from the engine and input to the engine) were computed by Eq. (2). The molar flow of each species was calculated by using Eq. (3). In this equation, $\dot{m}_{Inlet}$ and $\dot{m}_{Outlet}$ are equal to $\dot{m}_{Air}+\dot{m}_{Vapor}$ and $\dot{m}_{Air}+\dot{m}_{Vapor}+\dot{m}_{Injector}$, respectively, and M_W is the inlet or outlet mixture molecular mass.

$$\dot{n}_i=X_i\frac{\dot{m}_{Inlet\ or\ Outlet}}{M_{W,\ Inlet\ or\ Outlet}} \quad (3)$$

2.1.2. Enthalpy and entropy

Enthalpy and entropy were computed by using NASA equations and their constants. Eq. (4) and Eq. (5) are the NASA equations to calculate enthalpy and entropy at temperature T and Pressure 1 bar. The constants of Eq. (4) and Eq. (5) are obtained from NASA thermodynamic file [35].

$$\frac{h^{\circ}(T)}{\widetilde{R}}=-a_1T^{-1}+a_2ln(T)+a_3T+a_4\frac{T^2}{2}+a_5\frac{T^3}{3}+a_6\frac{T^4}{4}+a_7\frac{T^5}{5}+b_1 \quad (4)$$

$$\frac{s^{\circ}(T)}{\widetilde{R}}=-a_1\frac{T^{-2}}{2}-a_2T^{-1}+a_3ln(T)+a_4T+a_5\frac{T^2}{2}+a_6\frac{T^3}{3}+a_7\frac{T^4}{4}+b_2 \quad (5)$$

Eq. (4) is resulted by integrating C_P, so a reference temperature (absolute zero is suggested by NASA) must be used to calculate the actual enthalpy; the value $h^{\circ}(0)$ in Eq. (6) is obtained from NASA thermodynamic file. Eq. (7) is used to calculate the entropy of species i with partial pressure P_i.

$$h(T)=h^{\circ}(T)-h^{\circ}(0) \quad (6)$$

$$s(T,P_i)=s^{\circ}(T)-\widetilde{R}ln(P_i) \quad (7)$$

2.1.3. Chemical and thermophysical exergy

Eq. (8) and Eq. (9) were used to calculate thermophysical and chemical exergy [36], respectively. In these equations, H_i, S_i, and $P_{i,0}$ are equal to $\dot{n}_i{\cdot}h_i$, $\dot{n}_i{\cdot}s_i$, and $X_i{\cdot}P_0$, respectively. h_i, s_i, X_i, and $\psi^{\circ}_{Chem.,i}$ are enthalpy, entropy, molar fraction, and standard chemical exergy of species i in a mixture with m species and are computed by using Eq. (6), Eq. (7), Eq. (2), and Appendix A, respectively.

$$\Psi_{Th.Ph.}=\sum_{i=1}^{m}\left(H_i(T)-H_i(T_0)\right)-T_0\left(S_i(T,P_i)-S_i(T_0,P_{i,0})\right) \quad (8)$$

$$\Psi_{Chem.}=\sum_{i=1}^{m}\dot{n}_i\left(\psi^{\circ}_{Chem.,i}+\widetilde{R}\,T_0ln(X_i)\right) \quad (9)$$

2.1.4. Energy and exergy balance

In an engine, due to the combustion reaction, enthalpy of formation and total exergy (sum of thermophysical and chemical exergy) of the input and output mixtures should be used. The Energy and Exergy balance are shown in Eq. (10) and Eq. (11), respectively. In Eq. (10), the $H_f=\sum_{i=1}^{m}\dot{n}_ih_{f,i}$ is the enthalpy of formation for input or output mixture, W_{Net} is the indicated work, and Q_{Loss} is the heat transfer from the combustion chamber. The procedure to calculate h_f is described in Appendix A. In Eq. (11), the $\Psi_{Total}=\Psi_{Th.Ph.}+\Psi_{Chem.}$ is the total exergy for input or output mixture, $T_{Exchange}$ is the average inlet and outlet cooling water temperature, and $I_{Combustion}$ is the combustion irreversibility.

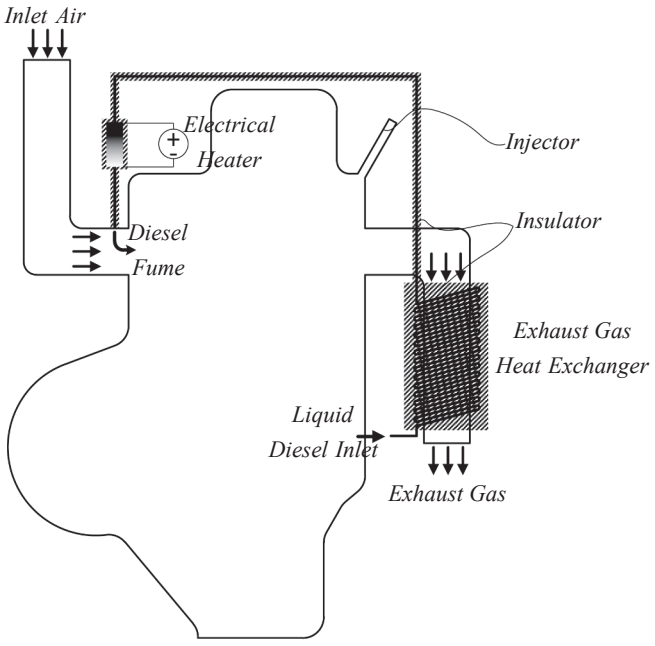

Fig. 1. Schematic of the proposed exhaust heat recovery.

$$H_{f,Inlet}-H_{f,Outlet}=W_{Net}+Q_{Loss} \quad (10)$$

$$\Psi_{Total,Inlet}-\Psi_{Total,Outlet}=W_{Net}+Q_{Loss}\left(1-\frac{T_0}{T_{Exchange}}\right)+I_{Combustion} \quad (11)$$

2.2. Cylinder pressure analysis

The environmental noise of the pressure signal was adjusted by the moving average smoothing method. Eq. (12) shows the relation among cylinder pressure (P), displaced volume ($V_{Displaced}$), and indicated mean effective pressure ($IMEP$). In Eq. (13), the $IMEP_i$ is the indicated mean effective pressure at the i cycle, $\overline{IMEP}$ is the average of $IMEP$ of all cycles, and COV is the coefficient of variation.

$$IMEP=\frac{\oint P\,dV}{V_{Displacement}} \quad (12)$$

$$COV_{IMEP}=\frac{\sqrt{\frac{\sum_{j=1}^{n}\left(IMEP_j-\overline{IMEP}\right)^2}{n}}}{\overline{IMEP}}\times 100 \quad (13)$$

In the first step of calculating the Heat Release Rate (HRR), the P-θ diagram average was calculated, then the HRR was resulted by using Eq. (14). In Eq. (14), γ is equal to 1.35 [37]. For calculating the Mass Fraction Burned (MFB), the Start of Ignition was assumed the point at which the HRR increases to more than zero, and the End of Ignition was considered the point at which the HRR decreases to less than zero. The MFB was calculated using Eq. (15), the angles of Start of Ignition and End of Ignition. In Eq. (15), MFB_j is the value of MFB up to angle θ_j. The crank angle of MFB50 was considered the point where MFB is equal to 50%. The angle of MFB50 is less dependent on the correct detection of the Start of Ignition, and it indicates the rapid homogeneous combustion.

$$HRR=\frac{\gamma}{\gamma-1}P\frac{dV}{d\theta}+\frac{1}{\gamma-1}V\frac{dP}{d\theta} \quad (14)$$

$$MFB_j=\frac{\int_{Start\ of\ Ignition}^{\theta_j}HRR(\theta)\,d\theta}{\int_{Start\ of\ Ignition}^{End\ of\ Ignition}HRR(\theta)\,d\theta} \quad (15)$$

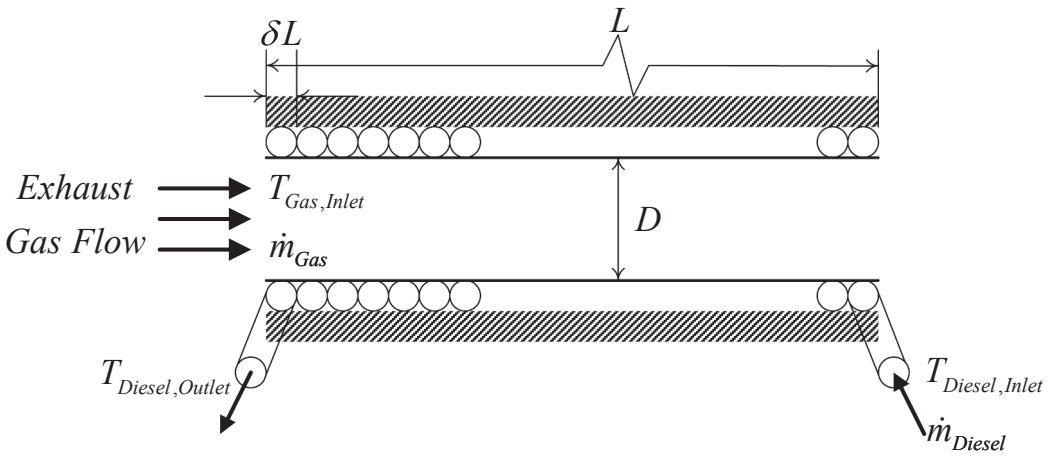

Fig. 2. Cropped view of the proposed heat exchanger.

2.3. Heat exchanger numerical analysis

The schematic of Fig. 1 was proposed to recover the energy of the exhaust gas to evaporate the diesel. In this design, a part of the exhaust pipe is replaced with a tube heat exchanger (Fig. 2). The exhaust gas energy is used for preheating or evaporating diesel before injecting it into the inlet duct. This design does not affect the exhaust gas pressure drop and will not harm the engine performance. In the heat exchanger, the experimentally-introduced Nusselt number correlation and the following algorithm were used to compute the heat transfer from the exhaust gas to the diesel.

- In each step, the exhaust gases transport properties were computed from the temperature and pressure of that step.
- The local Nusselt number was calculated using the introduced experimental relations (Eqs. (21) and (23)).
- According to the Nusselt number definition ($Nu = h_{Conv.}\, D/k$), the convection heat transfer coefficient was calculated. Also, The heat exchanger was assumed insulation ($Q_{HeatExchanger,Loss} = 0$); according to this, the heat transfer from the exhaust gas to diesel was computed.
- The diesel and the exhaust gas enthalpy in the next step were computed by the first law of thermodynamic ($Q_{Exchange} = H_{j+1} - H_j$).
- The diesel temperature and the exhaust gas mixture temperature in the next step were computed using Eq. (4) and the Newton-Raphson method.
- In the cross-flow heat exchanger, the outlet diesel's temperature was assumed to equal to the inlet exhaust gas. The above algorithm was repeated step by step until the diesel's temperature is equal to or lower than the preset temperature of inlet diesel. In this case, the required length of the heat exchanger is shorter than the preset size. If, until the last step, the diesel temperature does not reduce to the preset temperature of inlet diesel, then the temperature of outlet diesel was subtracted by 0.001 [*Kelvin*], and the solution algorithm was repeated.

2.3.1. Transport properties of a mixture

It is necessary to calculate the heat capacity at constant pressure, viscosity, and thermal conductivity of a gas mixture to calculate the Prandtl ($Pr = C_P\mu/k$) and Reynolds ($Re = \rho VD/\mu$) in the mixture. Eq. (16) is similar to Eqs. (4) and (5) with the same NASA constant; This equation was used to compute the heat capacity at constant pressure. The viscosity and Prandtl can be estimated using the relations introduced by Mansouri [38]. However, in this study, the mixture's thermal conductivity and viscosity were directly computed using the mixture's species transport properties. The transport properties of the exhaust gas species were directly obtained from the EES (Engineering Equation Solver) software. Eqs. (17) and (18) show the viscosity and the conductivity of a gas mixture with m species[39].

$$\frac{c_P(T)}{\widetilde{R}} = a_1T^{-2} + a_2T^{-1} + a_3 + a_4T + a_5T^2 + a_6T^3 + a_7T^4 \tag{16}$$

$$\mu_{Mix} = \sum_{i=1}^{m} \frac{X_i\,\mu_i}{X_i + \sum_{i=1}^{m} X_j\,M_{ij}} \tag{17}$$

$$k_{Mix} = \sum_{i=1}^{m} \frac{X_i\,k_i}{X_i + \sum_{i=1}^{m} X_j\,K_{ij}} \tag{18}$$

In Eqs. (17) and (18), M and K are the coefficients of interaction and have been calculated using Eqs. (19) and (20), respectively. In Eqs. (19) and (20), the μ_i, k_i, X_i, and $M_{W,i}$ are the viscosity, the conductivity, the molar fraction, and the i species molecular mass.

$$M_{ij} = \frac{1}{4}\left[1 + \left(\frac{\mu_i}{\mu_j}\right)^{1/2}\left(\frac{M_{W,j}}{M_{W,i}}\right)^{1/4}\right]^2\left(\frac{2M_{W,j}}{M_{W,i}+M_{W,j}}\right)^{1/2} \tag{19}$$

$$K_{ij} = M_{ij}\left[1 + \frac{2.41\left(M_{W,i}-M_{W,j}\right)\left(M_{W,i}-0.142M_{W,j}\right)}{\left(M_{W,i}+M_{W,j}\right)^2}\right] \tag{20}$$

2.3.2. Heat transfer coefficient

According to the Reynolds number in the exhaust pipe, the flow regime is completely turbulent ($Re > 10000$). Also, The Prandtl number is in the range of air ($Pr \approx 0.7$). For heat transfer in a turbulent internal flow, numerous empirical equations have been introduced in the literature. The Gnielinski correlation (Eq. (21)) provides the Nusselt number for the large Reynolds number range ($3000 \leqslant Re \leqslant 5\times10^6$), and it is valid for $0.5 \leqslant Pr \leqslant 2000$ [40]. Eq. (21) was used to calculate the convective heat transfer coefficient; in this equation, f is the friction factor and is calculated by Eq. (22) [41]. In Eq. (22), ε is the surface roughness and was considered 260×10^{-6}[*meter*] (cast iron) for the exhaust pipe. Also, D is the duct diameter and is equal to 7 cm for the exhaust pipe.

$$Nu_{Developed} = \frac{(f/8)(Re-1000)Pr}{1+12.7\sqrt{f/8}\left(Pr^{2/3}-1\right)} \tag{21}$$

$$\frac{1}{\sqrt{f}} = -2log\left(\frac{\varepsilon/D}{3.7} + \frac{2.51}{Re\sqrt{f}}\right) \tag{22}$$

Based on the exhaust pipe diameter in the studied engine, the development length is between 70 and 420 cm ($10D \leqslant z_{Fully\ Developed} \leqslant 60D$).

Table 2
Flow rates of injected fuel and percentage of vapor in the performed tests.

1000 rpm	Mass Flow of Injector [gr/sec]	0.21111				0.29729				0.40363		
	Percent of Vapor to Total Fuel	0	14.14	23.56	29.84	0	8.10	21.26	27.07	0	4.77	8.94	12.47

Table 3
Engine Specifications.

Parameter	Specification
Manufacturer	Perkins
Model	4.108
Bore	79.37 mm
Stroke	88.9 mm
No. of cylinders	4
Cubic capacity	1.760 lit
Compression ratio	22:1
Combustion system	Indirect Injection

Therefore, it is impossible to use Eq. (21) directly for a heat exchanger with a length of less than 70 cm. Eq. (23) has been introduced by Molki and Sparrow [42] for entrance length. At this equation, $\overline{Nu}$ ($= \frac{1}{L}\int_0^L Nu_z\, dz$) is the average Nusselt number from the inlet ($z = 0$) to the $z = L$.

$$\frac{\overline{Nu}}{Nu_{Developed}} = 1 + \frac{23.99Re^{-0.230}}{(L/D)^{-2.08\times10^{-6}Re+0.815}} \tag{23}$$

For calculating local Nusselt in each solution step, it was assumed that the Nusselt number is constant. So, in the first step, the average Nusselt number (Eq. (23)) was considered the local Nusselt number. In the second step, $\overline{Nu}$ is the average Nusselt number in the first and second step, so the second step local Nusselt number can be found. This process was repeated step by step until the end of the solution.

3. Experiment procedure

To investigate the diesel vapor effects on engine performance and emissions, diesel was evaporated in a closed cylinder, and the vapor was injected into the engine inlet air. The mass flow was calculated by weighing the cylinder at each test beginning and ending and dividing the test time. Due to the higher pressure of the vapor tank versus the inlet manifold, the diesel vapor easily streamed. A needle valve was used to control the diesel vapor flow rate. At a constant speed (1000 rpm), the amount of injector spray was set to three various values (corresponding to three different torques); in each case, the diesel vapor flow was adjusted to three different values. For comparison, the expressed results are shown in three loads (25, 50, and 75% of full load) and three vapor percentages (0, 5, 13, and 21% by mass of total fuel) by interpolating obtained results.

Table 2 shows the vapor percentage and the injector mass flow rate in experiments. Eq. (24) shows the relationship between the vapor percentage and the injector mass flow rate. In each test, after adjusting the speed and the diesel vapor and before collecting data, the engine was run for 5 min to make pretty sure that the engine condition is stable. In each test, cylinder pressure for 1000 consecutive cycles, soot level, exhaust gas emissions, fuel flow rate, and temperature of exhaust gas, inlet air, and inlet and outlet cooling water were recorded. For comparison of fumigation cases and non-fumigation cases at a constant load, by using interpolation of the originally recorded result at three loads of 25, 50, and 75 and three vapor percent of 5, 13, and 21, the final results were calculated and reported. The three loads of 25, 50 and, 75 are approximately equal to the average of the torque of four recorded data at three injection settings. The average torque in each injection setting is 14.925 N.m (21.321%), 33.325 N.m (47.607%), and 49.125 N.m (70.179%), respectively. Also, the maximum inlet vapor before knock at the maximum injection value studied is 12.48 ~ 13%, and the minimum inlet vapor whose effects can be recorded is 4.78 ~ 5%. So, the two vapor steps were selected. And due to the 8 percent difference between these two steps, the third step was selected as 21%.

Table 4
Accuracy and Uncertainty of Measured Parameters.

Parameter	Unit	Range	Resolution	Accuracy	Uncertainty
Torque	N.m	5–80	1	±1	±0.5
Speed	rpm	0–5000	1	±6	±0.0018
Temperature	°C	0–1370	0.1	±0.1%>	±0.05
Liquid Diesel Flowmeter	ml/sec	1–100	0.02	±0.5	±0.0099
Diesel Vapor Mass Measurement	gr	2–30000	2	±2	±1
Digital Stopwatch	sec	–	0.01	±0.01	±0.24
Soot	ppm	0–11276	0.2532	±2.62	±0.1264
CO	%vol	0–10	0.01	±0.03	±0.005
CO_2	%vol	0–20	0.1	±0.6	±0.5
O_2	%vol	0–21	0.01	±0.2	±0.005
HC as propane	ppm	0–5000	1	±20	±0.5
NO	ppm	0–5000	1	±10	±0.5
Cylinder Pressure	bar	0–300	0.03	±0.16	±0.015
Crank Angle	deg	0–360	0.36	±0.09	±0.18

Table 5
Consumed Fuel.

Parameter	Specification
Density	832 gr/lit
Final Bolling Point (FBP)	385 °C
Cetane Index	>49
Total Sulphur	<0.5 %w

$$Percent\ of\ Vapor\ to\ Total\ Fuel:\ VP = \frac{\dot{m}_{Vapor}}{\dot{m}_{Injector} + \dot{m}_{Vapor}} \times 100 \tag{240}$$

4. Experiment equipment

A four-cylinder engine manufactured by Perkins Co. was modified for the present study. The engine was coupled to a hydraulic dynamometer to control torque and speed. The engine specifications are shown in Table 3. The inlet and exhaust manifold temperatures and the inlet and outlet cooling water temperatures were measured every 100 ms over the time of each test by an ADAM-4018 + data logger. Their averages were used as the test inlet and exhaust manifold temperatures and the inlet and outlet cooling water temperatures. The volumetric airflow rate was measured using an orifice mounted on a surge tank. The volumetric flow rate of liquid diesel was measured by a burette, and it was converted to the mass flow rate by multiplying the density. An AVL 415 smoke meter and an MRU Delta1600 gas analyzer were used for the exhaust emissions measurement. The cylinder pressure was measured by an AVL-12QP-505CL sensor and a HICF-3059 amplifier. The cylinder pressure signal, the top dead center (TDC) pulse, and the crank angle pulse were recorded simultaneously by JIT-USB-4816 data logger with 480 kHz frequency and 16Bit resolution. The TDC position pulse and the crank angle pulse were generated by a HE50B-810006L5 encoder which generates 1000 pulses per revolution and one pulse for the TDC position. The accuracy and uncertainty of the instrument are listed in Table 4, and the uncertainty of the reported parameters is mentioned in Appendix B.

Diesel was heated in a 5-liter steel tank to a temperature of 386 °C by a 2000 W electric heater. The tank was covered with thick insulation of

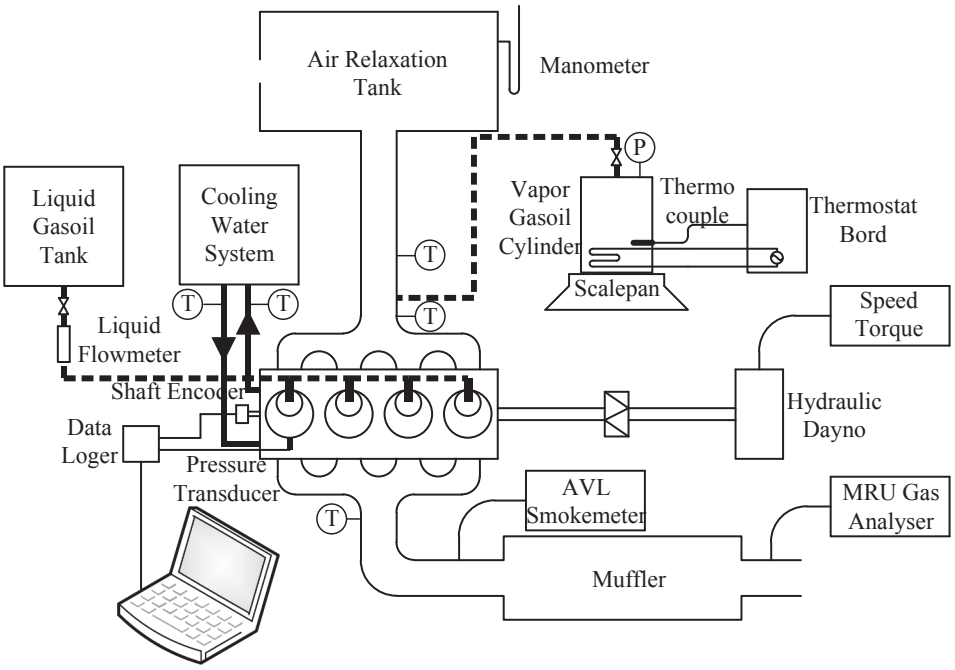

Fig. 3. The schematic of experimental equipment.

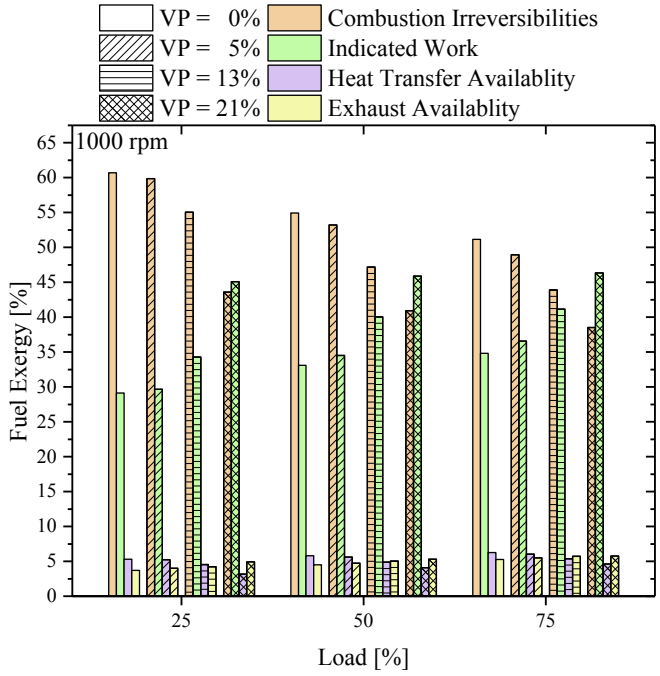

Fig. 4. The share of input exergy in the wasted exergy and the useful exergy, at three different loads and speed of 1000 rpm.

mineral wool to minimize heat loss. A thermostat regulated the tank temperature, and the tank pressure was always controlled to maintain safety. A steel needle valve was used to adjust the vapor flow rate. The tank was placed on a scalepan, and its instantaneous weight could be measured. The vapor pipeline was connected to the rubber pipe, which coupled the inlet manifold to the surge tank, for insulating scale from engine vibration. The consumed fuel is commercial diesel fuel with Euro 4 standard quality. Table 5 shows the characteristics of consumed diesel. Fig. 3 illustrates a schematic of the experimental equipment.

5. Results and discussions

5.1. Exergy analysis of engine

Fig. 4 shows the share of the indicated work, the exhaust gas, the heat transfer, and the combustion process irreversibility from engine inlet exergy. According to this figure, the largest share of exergy loss belongs to the combustion process, and the percentage of exergy loss through heat transfer is in the same order as the exergy output from the exhaust. In three studied loads, by increasing the diesel vapor share, the combustion irreversibility decreases and the percentage of indicated work increases. Also, heat transfer loss has been steadily reduced. Increasing the percentage of fuel vapor at a constant load increases the homogeneous combustion share; consequently, it reduces the maximum local temperature in the combustion chamber and, thus, reduces the exergy loss of heat transfer and combustion irreversibility. In a conventional compression combustion engine (like 0% of diese vapor), the fuel is injected into the hot air which is warm enough for auto-ignition of the fuel. The injected fuel is broken into tiny and coarse droplets. Some droplets absorb heat energy from the air and evaporate. Simultaneously, cylinder charge motion mixes the evaporated and non-evaporated fuel droplets with air. Due to the higher temperature of air than the auto-ignition temperature of the fuel, some premixed air–fuel packages burn (mostly with an equivalence ratio close to one). The ignition of premixed air–fuel packages increases the cylinder charge temperature and consequently evaporates other fuel droplets and makes more premixed air–fuel packages. In the meantime, due to the lack of sufficient oxygen in the vicinity of some droplets for combustion, those fuel droplets decompose to the constituent atoms (hydrogen and carbon) instead of combustion. The mixing of hot carbon particles with air and their diffusion combustion are parts of the combustion process. In the studied engine, some part of the fuel enters the cycle as vapor with intake air. The sufficient time for mixing the fuel vapor and the air (from the start of the compression stroke to the start of ignition), entering the fuel as vapor or distilled tiny droplets, and the lean fraction of fuel to air make a big diluted premixed air–fuel package. Whether the big diluted premixed air–fuel package is ignited by compression or is ignited by absorption of energy from the ignition of injected fuel, the combustion temperature of the big diluted premixed air–fuel package is certainly

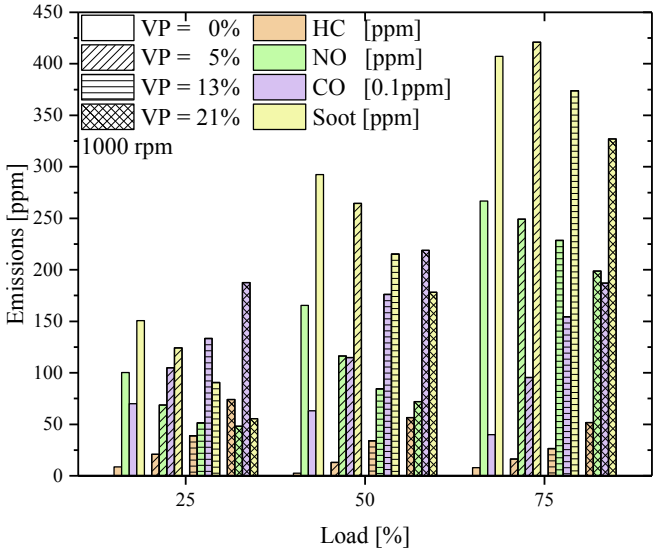

Fig. 5. The emissions of various pollutants in fumigation cases and non-fumigation cases, at three different loads and speed of 1000 rpm.

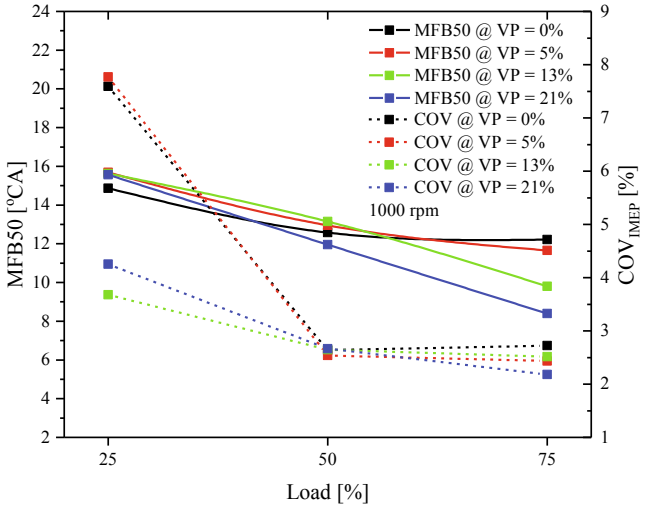

Fig. 6. MFB50 (left vertical axis) and COV_IMEP (right vertical axis) in fumigation cases and non-fumigation cases, at three different loads and speed of 1000 rpm.

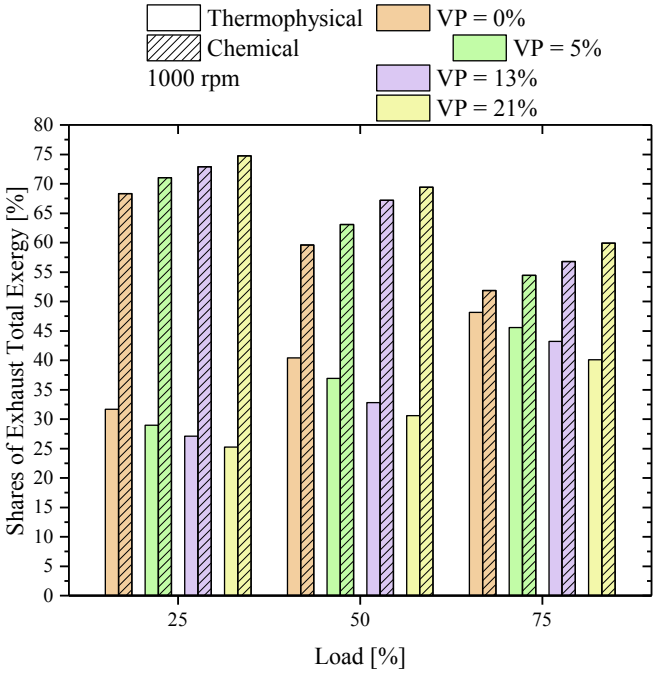

Fig. 7. The contribution of thermophysical and chemical exergy to the total exergy of exhaust gas, at three different loads and speed of 1000 rpm.

lower than the combustion temperature of the premixed air–fuel packages with an equivalence ratio close to one. Due to the placement of some air–fuel packages in the vicinity of the combustion chamber wall, the reduction of ignition temperature (reduction of local temperature) of these packages reduces the heat transfer losses. Despite the reduction of local temperature in the diluted premixed combustion, the average combustion chamber temperature relates to the pressure and volume of the combustion chamber and consequently IMEP. Therefore, at a constant load, the average combustion chamber temperature in premixed combustion is not significantly different from conventional combustion. As a result, the exhaust gas exergy does not significantly decrease or increase. The exergy of exhaust gas and indicated work are computed directly by measuring the molar fraction of exhaust gas and the cylinder pressure. However, as shown in Eqs. (10) and (11), and Appendix A, the combustion irreversibility and heat transfer depend on the diesel surrogate specifications. According to Fig. 4, the fuel conversion efficiency steadily increases while increasing the percentage of fuel vapor, so 21% w of diesel vapor gives the highest fuel conversion efficiency.

Fig. 5 illustrates the effects of fuel vapor on emitting carbon monoxide, nitrogen monoxide, soot, and unburned hydrocarbons. The addition of diesel vapor steadily decreases the nitrogen monoxide and soot emissions and simultaneously increases the carbon monoxide and unburned hydrocarbons emissions. Thus, the lowest nitrogen monoxide and soot emission level and the highest carbon monoxide and unburned hydrocarbon emission level are seen at 21% by mass of diesel vapor. The local temperature reduction and air–fuel proper mixing are the reasons that decrease the nitrogen monoxide and soot emissions, respectively. In convetional compression ignition, in the vicinity of the ignited premixed air–fuel packages (in homogeneous combustion phase) and ignited carbon particles (in mixing-controlled combustion phase), due to the high temperature of the flame cores, the nitrogen molecules of air decompose to their constituent atoms and it is the beginning of the NOx formation process. But in the adding diesel vapor condition, entering air and diesel vapor make a big diluted premixed air–fuel package. The combustion temperature of the big diluted premixed air–fuel package is certainly lower than the combustion temperature of the premixed air–fuel packages with an equivalence ratio close to one. It is one of the reasons that reduces the NOx emission in the case of adding diesel vapor. The penetration of fuel vapor into the crevices areas at the compression stroke and the lack of complete combustion of the fuel released from these areas in the expansion stroke are the reasons for increasing the emissions of unburned hydrocarbons and carbon monoxide. With increasing load, the nitrogen monoxide and soot emissions increase due to the increasing heavy hydrocarbons entering and the increasing combustion chamber local temperature, respectively. The soot formation is dependent on improper mixing and heavy hydrocarbons. Heavy hydrocarbons are part of the diesel fuel (as a mixture of different hydrocarbon). The homogeneous combustion of heavy hydrocarbon in diesel combustion process is not probable. So, most of the heavy hydrocarbon decomposes to its constructs atoms (carbon and hydrogen). The release of a large number of carbon particles is the the beginning of the soot formation process. With increasing load, the combustion chamber average temperature increases, so the unburned hydrocarbons emission reduces. Simultaneous with increasing load, the carbon monoxide emission is steadily decreasing at non-fumigation cases; but in fumigation cases, carbon monoxide emission is higher at 50% load than

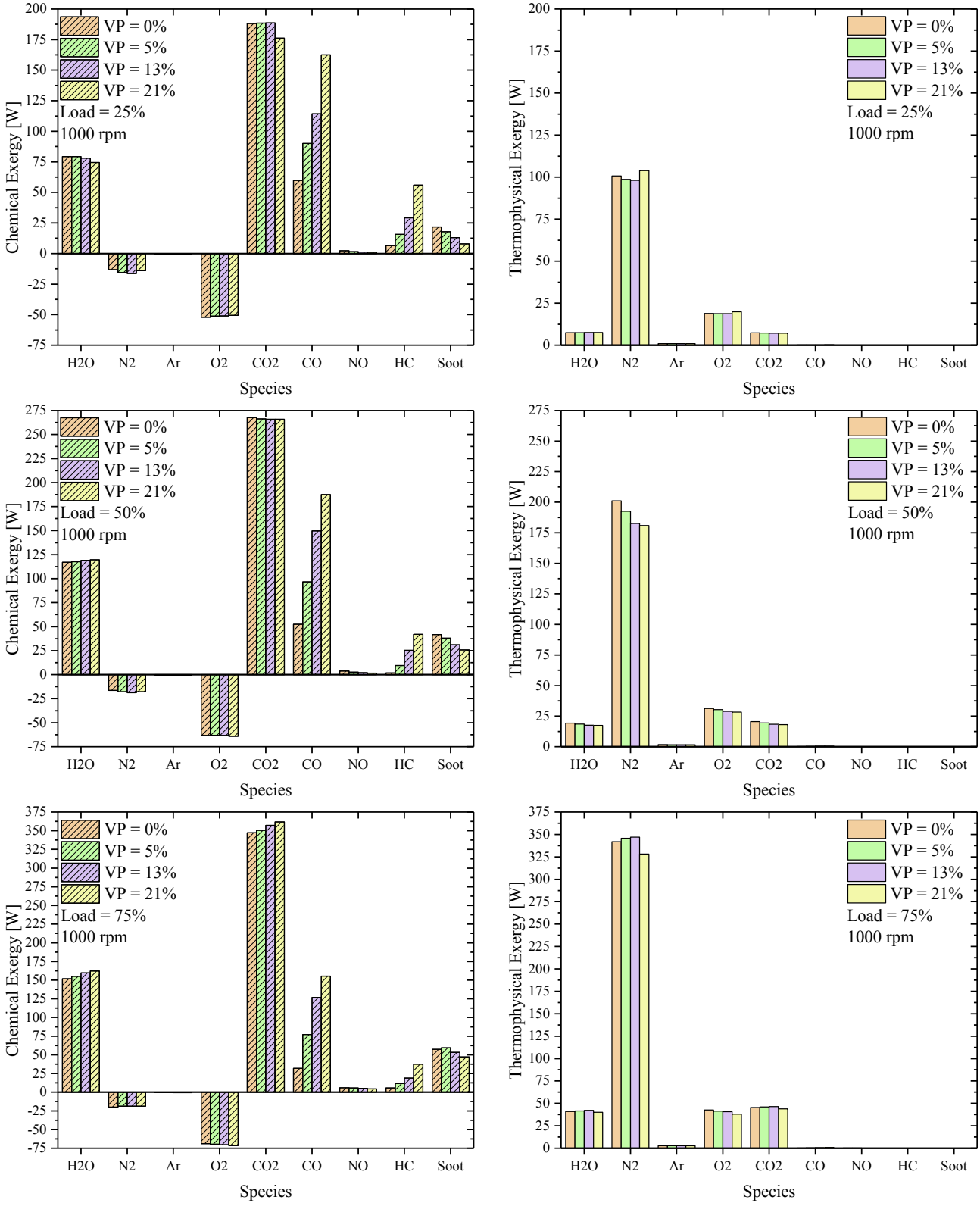

Fig. 8. Comparison of thermophysical and chemical exergy of various species, at three different loads and speed of 1000 rpm.

25 and 75% load. In fumigation cases, increasing carbon monoxide emissions from 25% load to 50% load and, then, decreasing from 50% load to 75% load is due to the interaction of two factors: the incomplete combustion of unburned hydrocarbons released from crevice areas and the increase of the average combustion chamber temperature. At 75% load, the effect of increasing combustion chamber temperature is more significant, and the carbon monoxide emission decreases. At 50% load, the impact of releasing unburned hydrocarbons from crevices areas is more substantial, and the carbon monoxide emission increases.

Fig. 6 illustrates MFB50 (left vertical axis) and COV_{IMEP} (right vertical axis) versus engine load. According to this figure, with increasing load, adding diesel vapor increases the rapid homogeneous combustion

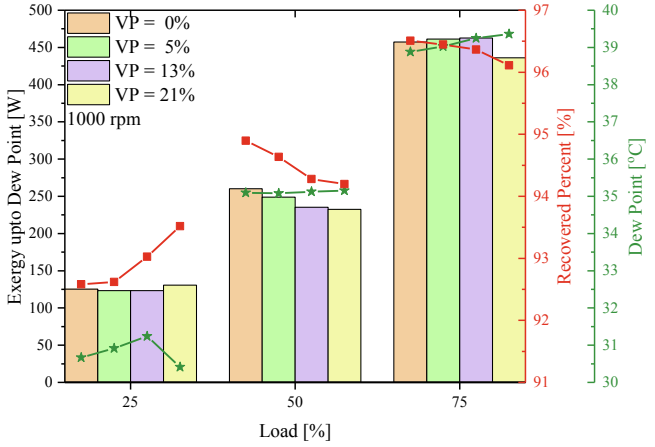

Fig. 9. Thermophysical exergy of exhaust gas to dew point (left axis), percentage of total thermophysical exergy recovery (right red axis), and dew point temperature (right green axis), at three different loads and speed of 1000 rpm.

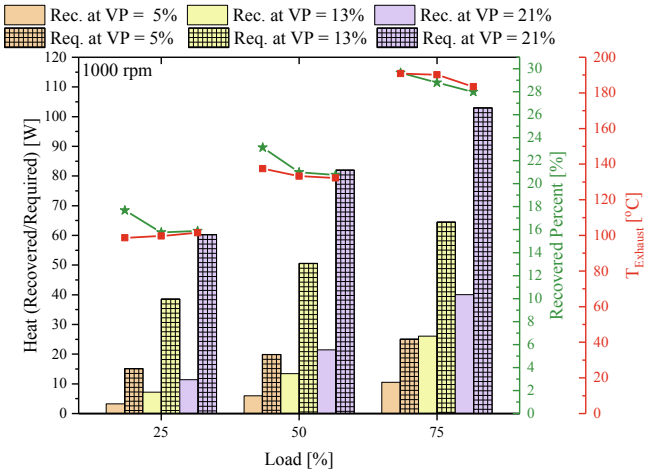

Fig. 10. Recovered (Rec.) heat from the exhaust gas if the diesel warms up to the temperature of the exhaust gas, and the Required (Req.) heat for evaporating diesel which has been warmed up to the exhaust gas temperature (left axis), the percentage of heat recovered to the total heat required (right green axis) and the temperature of the exhaust gas (right red axis), at three different loads and speed of 1000 rpm.

share. So, at 25% load, the MFB50 angle is advanced in non-fumigation cases from fumigation cases; by increasing load, the MFB50 angle is gradually retarded in non-fumigation cases of fumigation cases. The reason is the slower ignition of the dilute homogeneous mixture at 25% load. At 25% load and the fumigation cases, a part of the cycle energy supplies from dilute homogeneous mixture combustion. However, with increasing load and, consequently, increasing the entering vapor mass, the homogeneous air–fuel mixture concentration increases, so the rate of ignition increases.

According to Fig. 6, the COV decreases as the load increases. Also, the addition of diesel vapor in all three studied loads has reduced the COV. By comparison of the MFB50 and COV_{IMEP}, it can be said that the cycle variation decreases with increasing homogeneous combustion share, but the engine load is more effective than the homogeneous combustion share on the cycle variation. In compression ignition engines, reducing the engine load requires reducing the fuel injected into the combustion chamber. Therefore, at low loads, turbulent flows and residual gases have a more significant impact on the mixing process, the energy release rate, consequently the cycle variation. Adding diesel vapor, due to premixing the fuel and air, reduces the effect of the in-cylinder mixing process, which leads to a reduction in cycle variation.

Fig. 7 shows the contribution of thermophysical and chemical exergy to the total exergy of the exhaust gas. According to this figure, with increasing load and consequently increasing the temperature of exhaust gas, the share of thermophysical exergy increases, and simultaneously the share of chemical exergy decreases. Due to increasing carbon monoxide emissions and unburned hydrocarbons, increasing the percentage of diesel vapor increases chemical exergy share. According to Eqs. (9), (A2), and (A3), the chemical exergy of carbon monoxide and unburned hydrocarbons are higher than non-flammable species such as nitrogen monoxide due to their combustibility.

Fig. 8 shows the outlet thermophysical and chemical exergy of the species in the exhaust gas. According to this figure and Eq. (8), most of the thermophysical exergy is wasted by nitrogen and oxygen because these two species have the highest mole fraction among other species. Next, the carbon dioxide and water vapor have the highest molar fraction and consequently waste the most thermophysical exergy. Increasing load increases the exhaust gas temperature and the exhaust nitrogen thermophysical exergy, despite the constant airflow rate (due to the constant velocity and molar fraction of the exhaust nitrogen). Also, due to the increase of injected fuel as increasing load, the exhaust gas molar fraction of carbon dioxide and water vapor increases, although the molar fraction of oxygen decreases. Increasing load decreases the difference between the oxygen thermophysical exergy with the carbon dioxide and water vapor thermophysical exergy. And, they come approximately equal at 75% load, due to the cross effects of decreasing oxygen mole fraction and increasing exhaust gas temperature.

The concept of chemical exergy is the wasted work that destroys the environment. The environment chemical exergy is zero, and entering species with a concentration different from the concentration of that in the environment ruins the environment. According to the chemical exergy definition, its value can be negative or positive; but according to the chemical exergy concept, if it is not equal to zero, it means the destruction of the environment. Based on this concept, Fig. 8 has a different meaning from Fig. 5. The more significant environmental degradation is caused by carbon dioxide and water vapor emissions, which are directly related to combustion irreversibility (nature of the combustion reaction). Also, carbon monoxide, unburned hydrocarbons, and soot are more involved in environmental degradation than nitrogen monoxide. This can be explained by the combustibility of carbon monoxide, unburned hydrocarbons, and soot, which potentially waste

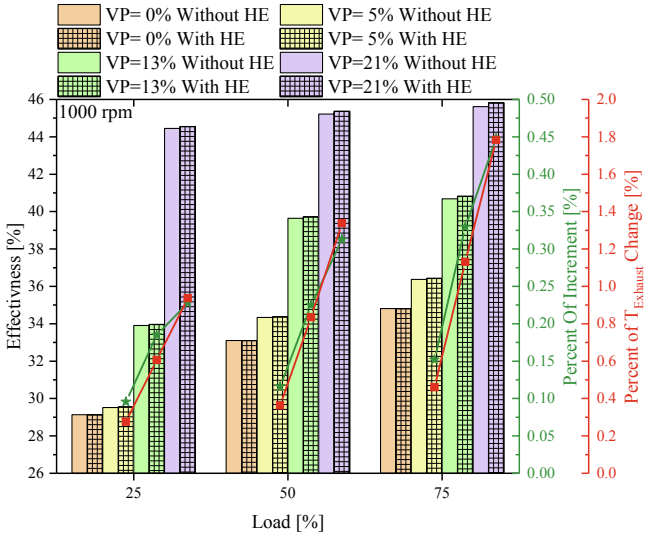

Fig. 11. The second law efficiency with the heat exchanger (HE) and without the heat exchanger (HE) (left axis), the percentage increase of the second law efficiency (right green axis), percentage of decrease in exhaust gas temperature (right red axis), at three different loads and speed of 1000 rpm.

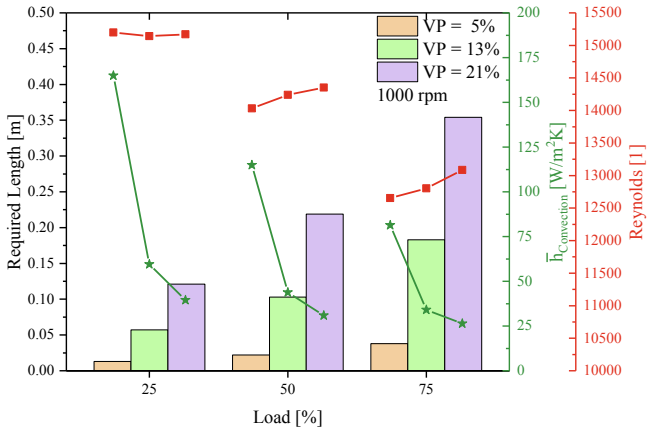

Fig. 12. The required length to increase diesel temperature from ambient temperature to exhaust gas temperature (left axis), average heat transfer rate during heating required (right green axis), and average Reynolds number for heating required (right red axis), at three different loads and speed of 1000 rpm.

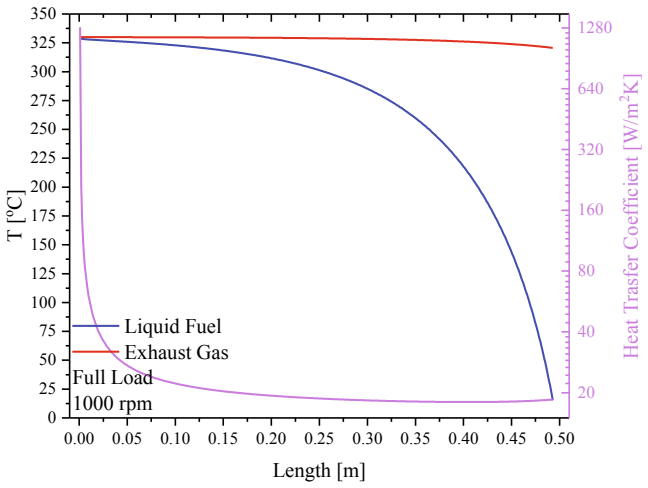

Fig. 13. Exhaust gas and diesel temperature variation along 50 cm length of HE and local heat transfer rate along the HE (right pink axis), at full loads and speed of 1000 rpm.

energy into the atmosphere.

5.2. Exhaust gas exergy recovery

One of the methods for improving efficiency is exhaust exergy recovery, which has a significant share of inlet fuel exergy as increasing load. In many recovery methods, the exhaust energy is recovered to the exhaust gas dew point. Fig. 4 shows the share of total exergy of exhaust gas, and Fig. 9 shows the thermophysical exergy of exhaust gas to the dew point of the mixture. As shown in Fig. 9, the exhaust exergy down to dew point includes 91% of the exhaust gas thermophysical exergy. According to Fig. 7, the exhaust gas thermophysical exergy comprises 30–50% of total exhaust exergy. Increasing load raises the exhaust gas dew point. In each step (from 25% to 50% and from 50% to 75%), the dew point rises approximately 4 °C. Increasing load augments the burned fuel mass, so the molar fraction of water vapor in the exhaust mixture increases. At a constant load, the dew point fluctuates approximately 0.5–1 °C. These fluctuations are due to the interaction of two (positive and negative) effects: increasing the fuel conversion efficiency and the CO emission. Increasing CO emission leads to the production of water, based on the following reaction: $CO_2 + H_2 \rightarrow CO + H_2O$.

Fig. 10 shows the Recovered (Rec.) heat from the exhaust gas if the diesel warms up to the exhaust gas temperature and the Required (Req.) heat for evaporating diesel which has been warmed up to the exhaust gas temperature. At a constant load, despite approximately constant exhaust temperature, the recovered heat increases simultaneously with increasing fuel vapor percentage due to the increasing diesel vapor flow. The recovered heat percentage rises from 16% at 5% diesel vapor to 30% at 21% diesel vapor. Increasing load from 25% to 75% increases the exhaust gas temperature from 100 °C to 190 °C. Also, adding diesel vapor decreases the exhaust gas temperature between 1 and 5 °C. By comparing recovered heat at different loads with equal vapor percentage, it can be concluded that, due to increasing the vapor flow and the exhaust temperature, the recovered heat rises. According to Fig. 10, because the exhaust gas temperature is lower than the diesel final boiling point (385 °C), most of the required heat of diesel evaporation should be supplied by an electrical heater.

Fig. 11 shows the second law efficiency (η_{II}) with and without Heat Exchanger (HE). According to this figure, increasing fuel vapor increases η_{II}, and using 21% fuel vapor gives the highest η_{II}. Also, using fuel vapor increases the maximum η_{II} from 32% to 43%. The exhaust heat recovery has no significant effect on increasing η_{II}due to the low flow rate of diesel vapor, which could not recover a considerable amount of exergy. The HE outlet gas has high temperature and high availability, which could be retrieved in a downstream thermal cycle. Using HE improves η_{II} by a maximum of 0.45% and reduces the exhaust gas temperature by a maximum of 1.8%.

Fig. 12 shows the required length of HE to increase diesel temperature from the ambient temperature to the exhaust temperature; also, the average Reynolds number and the convective heat transfer coefficient ($\overline{h_{Conv.}}$) in the required length are shown. According to the average Reynolds number, the exhaust pipe flow regime is turbulent, so using Eq.21 is correct. Due to the development of flow, the $\overline{h_{Conv.}}$ reduces by increasing the required length. Increasing fuel vapor increases the necessary length due to increasing inlet diesel flow of HE. Decreasing exhaust gas temperature changes the exhaust gas viscosity and density, so the Reynolds number changes along the HE. According to Fig. 12, the Reynolds number slightly reduces by increasing the required length of the HE. The adequate HE length for recovering heat from the exhaust gas is the maximum required HE length. According to Fig. 12, an HE with 35 cm length can recover heat from exhaust gas to increase diesel temperature from ambient temperature to the exhaust temperature at load range up to 75% and fuel vapor range up to 21%.

Extrapolation was used to calculate the exhaust gas temperature and the diesel vapor flow rate at full load and 21% fuel vapor to predict the HE length needed. Fig. 13 shows the variation of the exhaust gas temperature, the diesel temperature, and the local convective heat transfer coefficient along the length of HE at full load. According to Fig. 13, a 50 cm heat exchanger can increase the diesel temperature from 15 °C to 330 °C and simultaneously reduce the exhaust gas temperature from 330 °C to 320 °C. At full load, the HE can recover 45% of the required energy of evaporation.

6. Conclusions

In this study, the effects of adding diesel vapor on the useful and wasted exergy as well as exhaust emissions were investigated. In order to achieve this goal, the tests were performed at a constant speed of 1000 rpm. The speed of 1000 rpm has been chosen as the lowest operating speed of the studied engine. And, due to this fact, it's the best speed to see the effects of premixed combustion. As the engine knock tendency increases by decreasing speed, the choice of 1000 rpm, as the lowest researchable speed, proves the possibility of adding diesel vapor at a higher speed. At the constant speed, the injected fuel was increased in three steps. And, in each fuel injection step, the amount of diesel vapor was increased in three steps up to the knock threshold. After recording the raw data, for comparing the engine performance with and without diesel vapor, the results were calculated by interpolating the raw data at

three loads of 25, 50, and 75% (of full load) and three vapor percent of 5, 13, and 21% (of total entered fuel). Also, a numerical analysis was performed on recovering energy and exergy of exhaust gas for evaporating diesel. A summary of the obtained results is listed below:

- The added diesel vapor into the intake air makes a diluted homogeneous air–fuel mixture in the compression stroke. The ignition of this diluted homogeneous mixture supplies a part of cycle combustion energy. Therefore, adding diesel vapor increases the share of homogeneous combustion.
- The ignition temperature of the diluted homogeneous air–fuel mixture is lower than the ignition temperature of injected fuel in the conventional diesel engine. This means the local temperature decreases, and reducing the local temperature in the combustion process decreases the combustion irreversibility and heat transfer exergy loss. Therefore, adding diesel vapor increases combustion efficiency.
- Despite the reduction of the local temperature by increasing the share of homogeneous combustion, the average temperature of the combustion chamber remains constant, due to the dependence of the average temperature of the combustion chamber on the engine load. Therefore, adding diesel vapor has no significant effect on exhaust gas temperature. And, due to the speed and load being constant, the exhaust gas exergy has no significant change by adding diesel vapor.
- The effects of adding diesel vapor on exhaust emissions are so close to other homogeneous combustion (HCCI, PCCI, and RCCI), which reduces NO and PM and increases CO and HC. The reducing local temperature decreases the NOx formation. Also, the well-mixed air–fuel vapor reduces soot (PM) emission. But due to the presence of fuel vapor in the compression stroke, the fuel vapor enters into the crevices areas, and the emission of HC and CO increases.
- According to achieved results, adding diesel vapor decreases the cyclic variation. Adding diesel vapor increases the share of homogeneous combustion and decreases the share of mixing-controlled combustion. So, adding diesel vapor reduces the effects of the in-cylinder mixing process as one of the most important factors in cyclic variation.
- The concept of chemical exergy is the work that is wasted to destroy the environment. The environment chemical exergy is zero, and entering species with a concentration different from the concentration of that in the environment ruins the environment. According to the species chemical exergy investigation in details, the CO2 and H2O emissions and O2 consumption have the most environmentally-destructive effect. In the second place, the CO emission has the most environmentally-damaging impact. And, adding diesel vapor increases the adverse effect of emitting CO and HC in environmental destruction. This can be explained by the combustibility of carbon monoxide, and unburned hydrocarbons which potentially waste energy into the atmosphere.
- In most industrial recovery of energy from the combustion products, the energy recovery continues until the product's water is not distilled. So, the dew point of the exhaust mixture was chosen as the lowest temperature for energy recovery. The exhaust gas thermophysical exergy down to the dew point comprises more than 90% of the total exhaust gas thermophysical exergy. The increasing load increases the dew point, but, due to the rising exhaust temperature, the exhaust gas thermophysical exergy share down to the dew point increases.
- In the compression combustion engine, the exhaust gas temperature depends on the engine load. At low load, the exhaust gas temperature may not be high enough for evaporating diesel fuel. According to achieved results, using a heat exchanger (HE) on the exhaust pipe can recover 20–30% of the required heat for evaporating diesel. Increasing load increases recovered heat. Based on the experimentally recorded data and the extrapolation, the exhaust gas temperature at full load and 21% of diesel vapor was calculated. At full load, a 50 cm length HE can warm up diesel from ambient temperature to exhaust gas temperature. Also, at full load, approximately 45% of the required heat for evaporating diesel is recovered.
- Adding diesel vapor increases second law efficiency from 30% to 44%. Adding 21% diesel vapor has the most positive effects on fuel conversion efficiency, NO emission, and soot emission. Using an HE in this proposal has not significantly improved second law efficiency due to the low flow rate of diesel which does not considerably retrieve the recoverable heat.

CRediT authorship contribution statement

Mohsen Bashi: Conceptualization, Methodology, Software, Writing - original draft, Investigation. **Mohsen Ghazikhani:** Supervision, Resources, Writing - review & editing.

Declaration of Competing Interest

The authors declare that they have no known competing financial interests or personal relationships that could have appeared to influence the work reported in this paper.

Appendix A

The standard chemical exergy of atmospheric species can be calculated using Table 1 and Eq. A(1) [36]. Eq. A(1) is a function of the ambient temperature and environment species molar fraction, which according to Table 1, is a function of relative humidity.

$$\psi^{\circ}_{Chem.,i} = \widetilde{R}\, T_0 ln\left(x_{i,e}\right) \tag{A1}$$

The standard chemical exergy of species at a specific environmental condition is mentioned in the literature [43,44], but Eq. A(1) calculates the standard chemical exergy at an arbitrary environmental condition. The standard chemical exergy is a function of the chemical potential of various elements and compounds in nature (depending on their concentration in nature). Many compounds do not exist in nature; in such cases, a reaction can be defined based on compounds and elements in nature so that its product is the unknown compound. The standard chemical exergy of the unknown compound can be calculated by balancing the standard chemical exergy and the Gibbs energy of formation of the reactants and the products (Eq. (A2)).

$$\sum_{Product} x_i \psi^{\circ}_{Chem.,i} - \sum_{Reactant} x_i \psi^{\circ}_{Chem.,i} = \sum_{Product} x_i g_{f,i} - \sum_{Reactant} x_i g_{f,i} \tag{A2}$$

In Eq. (A2), g_f is the Gibbs energy of formation. The Gibbs energy of formation for any element and compound can be calculated, and it is equal to zero at the standard condition ($P = 1\ bar,\ T = 25\ ^{\circ}C$) for elements. Eq. (A3) is used to calculate Gibbs energy of formation for compounds and elements at the non-standard condition. It should be noted that in a formation reaction of an unknown compound, elements are reacted as the reactant, and only the unknown compound is achieved. Based on the same reaction of formation and Eq. (A4), the enthalpy of formation can be calculated. In Eq. (A3) and Eq. (A4), the h° and the s° are computed using Eqs. (4) and (5), respectively.

$$g_{f,Product} = h^{\circ}_{Product} - \sum_{Reactant} x_i h^{\circ}_i - T_0\left(s^{\circ}_{Product} - \sum_{Reactant} x_i s^{\circ}_i\right) \tag{A3}$$

$$h_{f,Product} = h^{\circ}_{Product} - \sum_{Reactant} x_i h^{\circ}_i \tag{A4}$$

Appendix B

If the function f depends on independent variable $x_1, x_2, \ldots, x_n$, and the uncertainty of the independent variables are $\delta x_1, \delta x_2, \ldots, \delta x_n$, then the uncertainty of f is shown by Eq. B(1) [45].

$$\delta f = \sqrt{\left(\frac{\partial f}{\partial x_1}\delta x_1\right)^2 + \left(\frac{\partial f}{\partial x_2}\delta x_2\right)^2 + \cdots + \left(\frac{\partial f}{\partial x_n}\delta x_n\right)^2} \tag{B1}$$

Table B1
Uncertainty Equations Table.

$$\delta\Psi_{Th.Ph.,i} = \sqrt{\left(\psi_{Th.Ph.,i}\delta\dot{n}_i\right)^2 + \left[\dot{n}_i\left(\frac{\partial h_i}{\partial T} - T_0\frac{\partial s_i}{\partial T}\right)\delta T\right]^2 + \left[\dot{n}_i T_0\frac{\partial s_i}{\partial P}\delta P\right]^2}$$

$$\delta\Psi_{Chem.,i} = \sqrt{\left(\dot{n}_i\left(\widetilde{R}T_0/X_i\right)\delta X_i\right)^2 + \left(\psi_{Chem.,i}\delta\dot{n}_i\right)^2}$$

$$\delta\Psi_{Total} = \sqrt{\sum \delta\Psi^2_{Th.Ph.,i} + \delta\Psi^2_{Chem.,i}}$$

$$\delta Q_{Loss} = \sqrt{\delta W^2_{Net} + \sum_{Intake}\left(\dot{n}_i\delta h_{f,i}\right)^2 + \left(h_{f,i}\delta\dot{n}_i\right)^2 + \sum_{Outlet}\left(\dot{n}_i\delta h_{f,i}\right)^2 + \left(h_{f,i}\delta\dot{n}_i\right)^2}$$

$$\delta Exergy_{Q_{Loss}} = \left(1 - \frac{T_0}{T_{Exchange}}\right)\delta Q_{Loss}$$

$$\delta I_{Combustion} = \sqrt{\delta\Psi^2_{Total,Inlet} + \delta\Psi^2_{Total,Outlet} + \delta W^2_{Net} + \left(1 - \frac{T_0}{T_{Exchange}}\right)^2\delta Q^2_{Loss}}$$

$$\delta W_{Net} = \frac{1}{\sqrt{2}}\sqrt{\sum\left(V_{j+1} - V_j\right)^2\delta P^2 + \left(P_j + P_{j+1}\right)^2\delta V^2}$$

$$\delta COV_{IMEP} = \sqrt{\frac{1}{n} + COV^2_{IMEP}}\ \frac{\delta IMEP}{\overline{IMEP}}$$

$$\delta MFB50 = \delta\theta$$

Table B2
Uncertainty of Parameters that were Shown in Results Section.

Parameter	Uncertainty	Uncertainty percentage
$\delta\Psi_{Th.Ph.\ Exhaust}$	3.3650 [W]	$\delta\Psi_{Th.Ph.\ Exhaust}/\Psi_{Total\ Intake} = 0.1712$ %
δW_{Net}	19.0304 [W]	$\delta W_{Net}/\Psi_{Total\ Intake} = 0.1242$ %
$\delta Exergy_{Q_{Loss}}$	107.2966 [W]	$\delta Exergy_{Q_{Loss}}/\Psi_{Total\ Intake} = 0.6913$ %
$\delta I_{Combustion}$	112.0558 [W]	$\delta I_{Combustion}/\Psi_{Total\ Intake} = 0.7233$ %
$\delta\Psi_{Chem.\ Exhaust}$	25.5845 [W]	$\delta\Psi_{Cehm.\ Exhaust}/\Psi_{Total\ Exhaust} = 3.7774$ %
$\delta\Psi_{Total\ Exhaust}$	25.8496 [W]	$\delta\Psi_{Th.Ph.\ Exhaust}/\Psi_{Total\ Exhaust} = 0.4106$ %
δQ_{Loss}	893.9716 [W]	$\delta Q_{Loss}/\left(H_{f,Intake} - H_{f,Exhaust}\right) = 7.7504$ %
δCOV_{IMEP}	1.25 [%]	–
$\delta MFB50$	0.18 [deg]	–
$\delta\Psi_{Th.Ph.\ H2O}$	0.3557 [W]	$\delta\Psi_{Th.Ph.\ H2O}/\Psi_{Th.Ph.\ Exhaust} = 0.1822$ %
$\delta\Psi_{Th.Ph.\ N2}$	0.6382 [W]	$\delta\Psi_{Th.Ph.\ N2}/\Psi_{Th.Ph.\ Exhaust} = 0.3269$ %
$\delta\Psi_{Th.Ph.\ Ar}$	0.0138 [W]	$\delta\Psi_{Th.Ph.\ Ar}/\Psi_{Th.Ph.\ Exhaust} = 0.0071$ %
$\delta\Psi_{Th.Ph.\ O2}$	0.1178 [W]	$\delta\Psi_{Th.Ph.\ O2}/\Psi_{Th.Ph.\ Exhaust} = 0.0603$ %
$\delta\Psi_{Th.Ph.\ CO2}$	0.4050 [W]	$\delta\Psi_{Th.Ph.\ CO2}/\Psi_{Th.Ph.\ Exhaust} = 0.2074$ %
$\delta\Psi_{Th.Ph.\ CO}$	0.0031 [W]	$\delta\Psi_{Th.Ph.\ CO}/\Psi_{Th.Ph.\ Exhaust} = 0.0016$ %
$\delta\Psi_{Th.Ph.\ NO}$	0.000062 [W]	$\delta\Psi_{Th.Ph.\ NO}/\Psi_{Th.Ph.\ Exhaust} = 3.1727 \times 10^{-5}$ %
$\delta\Psi_{Th.Ph.\ HC}$	0.000126 [W]	$\delta\Psi_{Th.Ph.\ HC}/\Psi_{Th.Ph.\ Exhaust} = 6.4723 \times 10^{-5}$ %
$\delta\Psi_{Th.Ph.\ Soot}$	0.000014 [W]	$\delta\Psi_{Th.Ph.\ Soot}/\Psi_{Th.Ph.\ Exhaust} = 7.2989 \times 10^{-6}$ %
$\delta\Psi_{Chem.\ H2O}$	7.5170 [W]	$\delta\Psi_{Chem.\ H2O}/\Psi_{Chem.\ Exhaust} = 1.6570$ %
$\delta\Psi_{Chem.\ N2}$	5.8929 [W]	$\delta\Psi_{Chem.\ N2}/\Psi_{Chem.\ Exhaust} = 1.2990$ %
$\delta\Psi_{Chem.\ Ar}$	0.2682 [W]	$\delta\Psi_{Chem.\ Ar}/\Psi_{Chem.\ Exhaust} = 0.0591$ %
$\delta\Psi_{Chem.\ O2}$	0.8867 [W]	$\delta\Psi_{Chem.\ O2}/\Psi_{Chem.\ Exhaust} = 0.1955$ %
$\delta\Psi_{Chem.\ CO2}$	21.3613 [W]	$\delta\Psi_{Chem.\ CO2}/\Psi_{Chem.\ Exhaust} = 4.7088$ %
$\delta\Psi_{Chem.\ CO}$	4.3816 [W]	$\delta\Psi_{Chem.\ CO}/\Psi_{Chem.\ Exhaust} = 0.9658$ %
$\delta\Psi_{Chem.\ NO}$	0.0226 [W]	$\delta\Psi_{Chem.\ NO}/\Psi_{Chem.\ Exhaust} = 0.0050$ %
$\delta\Psi_{Chem.\ HC}$	0.5838 [W]	$\delta\Psi_{Chem.\ HC}/\Psi_{Chem.\ Exhaust} = 0.1287$ %
$\delta\Psi_{Chem.\ Soot}$	0.0900 [W]	$\delta\Psi_{Th.Ph.\ Soot}/\Psi_{Th.Ph.\ Exhaust} = 0.0198$ %

According to the introduced equations in the manuscript, the following equation table (Table B1) is represented to calculate the reported parameters' uncertainty. To prove these equations, it's assumed that T_0, P_0, ϕ, and ψ°_{Chem} are exact and have no uncertainty. Also in parameters that have numerical integral, the numerical integral method was assumed trapezoidal method. According to the uncertainty equation table, the uncertainty of each parameter depends on its value. Hence the uncertainty is reported based on the average value calculated using the recorded raw data. The uncertainty (values) and percentage uncertainty of parameters that were shown in the result section are shown in Table B2.

References

[1] World Energy Balances n.d. https://www.iea.org/subscribe-to-data-services/world-energy-balances-and-statistics.

[2] CO2 Emissions from Fuel Combustion n.d. https://www.iea.org/subscribe-to-data-services/co2-emissions-statistics.

[3] Setti L, Passarini F, De Gennaro G, Barbieri P, Perrone MG, Borelli M, et al. SARS-Cov-2RNA found on particulate matter of Bergamo in Northern Italy: First evidence. Environ Res 2020;188:109754. https://doi.org/10.1016/j.envres.2020.109754.

[4] Liu S, Li M. Ambient air pollutants and their effect on COVID-19 mortality in the United States of America. Rev Panam Salud Publica/Pan Am J Public Heal 2020;44:1–6. https://doi.org/10.26633/RPSP.2020.159.

[5] Konstantinoudis G, Padellini T, Bennett J, Davies B, Ezzati M, Blangiardo M. Long-term exposure to air-pollution and COVID-19 mortality in England: A hierarchical spatial analysis. Environ Int 2021;146:106316. https://doi.org/10.1016/j.envint.2020.106316.

[6] Onishi S, Jo SH, Shoda K, Jo PD, Kato S. Active Thermo-Atmosphere Combustion (ATAC) - A New Combustion Process for Internal Combustion Engines 1979. https://doi.org/10.4271/790501.

[7] Aoyama T, Hattori Y, Mizuta J, Sato Y. An experimental study on premixed-charge compression ignition gasoline. Engine 1996. https://doi.org/10.4271/960081.

[8] Kokjohn SL, Hanson RM, Splitter DA, Reitz RD. Fuel reactivity controlled compression ignition (RCCI): a pathway to controlled high-efficiency clean combustion. Int J Engine Res 2011;12(3):209–26. https://doi.org/10.1177/1468087411401548.

[9] Duan X, Lai M-C, Jansons M, Guo G, Liu J. A review of controlling strategies of the ignition timing and combustion phase in homogeneous charge compression ignition (HCCI) engine. Fuel 2021;285:119142. https://doi.org/10.1016/j.fuel.2020.119142.

[10] Shim E, Park H, Bae C. Comparisons of advanced combustion technologies (HCCI, PCCI, and dual-fuel PCCI) on engine performance and emission characteristics in a heavy-duty diesel engine. Fuel 2020;262:116436. https://doi.org/10.1016/j.fuel.2019.116436.

[11] Singh AP, Kumar V, Agarwal AK. Evaluation of comparative engine combustion, performance and emission characteristics of low temperature combustion (PCCI and RCCI) modes. Appl Energy 2020;278:115644. https://doi.org/10.1016/j.apenergy.2020.115644.

[12] Paykani A, Garcia A, Shahbakhti M, Rahnama P, Reitz RD. Reactivity controlled compression ignition engine: Pathways towards commercial viability. Appl Energy 2021;282:116174. https://doi.org/10.1016/j.apenergy.2020.116174.

[13] Mohan B, Yang W, Chou S, kiang. Fuel injection strategies for performance improvement and emissions reduction in compression ignition engines—A review. Renew Sustain Energy Rev 2013;28:664–76. https://doi.org/10.1016/j.rser.2013.08.051.

[14] Bharathiraja M, Venkatachalam R, Senthilmurugan V. Performance, emission, energy and exergy analyses of gasoline fumigated DI diesel engine. J Therm Anal Calorim 2019;136(1):281–93. https://doi.org/10.1007/s10973-018-7933-0.

[15] Şahin Z, Durgun O, Kurt M. Experimental investigation of improving diesel combustion and engine performance by ethanol fumigation-heat release and flammability analysis. Energy Convers Manag 2015;89:175–87. https://doi.org/10.1016/j.enconman.2014.09.053.

[16] Abedin MJ, Masjuki HH, Kalam MA, Sanjid A, Rahman SMA, Masum BM. Energy balance of internal combustion engines using alternative fuels. Renew Sustain Energy Rev 2013;26:20–33. https://doi.org/10.1016/j.rser.2013.05.049.

[17] Marami Milani S, Khoshbakhti Saray R, Najafi M. Comparison of different optimized heat driven power-cycle configurations of a gas engine. Appl Therm Eng 2020;179:115768. https://doi.org/10.1016/j.applthermaleng.2020.115768.

[18] Zhu S, Ma Z, Zhang K, Deng K. Energy and exergy analysis of a novel steam injected turbocompounding system applied on the marine two-stroke diesel engine. Energy Convers Manag 2020;221:113207. https://doi.org/10.1016/j.enconman.2020.113207.

[19] Zhu S, Zhang K, Deng K. A review of waste heat recovery from the marine engine with highly efficient bottoming power cycles. Renew Sustain Energy Rev 2020;120:109611. https://doi.org/10.1016/j.rser.2019.109611.

[20] Ouyang T, Huang G, Su Z, Xu J, Zhou F, Chen N. Design and optimisation of an advanced waste heat cascade utilisation system for a large marine diesel engine. J Clean Prod 2020;273:123057. https://doi.org/10.1016/j.jclepro.2020.123057.

[21] Thaddaeus Julius, Unachukwu Godwin, Mgbemene Chigbo, Mohammed Ahmed, Pesyridis Apostolos. Overview of recent developments and the future of organic Rankine cycle applications for exhaust energy recovery in highway truck engines. Int J Green Energy 2020;17(15):1005–21. https://doi.org/10.1080/15435075.2020.1818247.

[22] Ravi R, Pachamuthu S. Experimental investigation on innovatory waste heat recovery system impacts on DIESEL engine exhaust emissions. Energy Sources, Part A Recover Util Environ Eff 2020;1–24. https://doi.org/10.1080/15567036.2020.1758247.

[23] Ravi R, Pachamuthu S, Kasinathan P. Computational and experimental investigation on effective utilization of waste heat from diesel engine exhaust using a fin protracted heat exchanger. Energy 2020;200:117489. https://doi.org/10.1016/j.energy.2020.117489.

[24] Instruction manual of DELTA 1600S-IV.

[25] Smoke Value Measurment with the Filter Paper Method; 2005.

[26] Patel A, Kong S-C, Reitz RD. Development and Validation of a Reduced Reaction Mechanism for HCCI Engine Simulations 2004. https://doi.org/10.4271/2004-01-0558.

[27] Wang H, Ra Y, Jia M, Reitz RD. Development of a reduced n-dodecane-PAH mechanism and its application for n-dodecane soot predictions. Fuel 2014;136:25–36. https://doi.org/10.1016/j.fuel.2014.07.028.

[28] Wang H, Deneys Reitz R, Yao M, Yang B, Jiao Q, Qiu L. Development of an n-heptane-n-butanol-PAH mechanism and its application for combustion and soot prediction. Combust Flame 2013;160:504–19. https://doi.org/10.1016/j.combustflame.2012.11.017.

[29] Wang Hu, Jiao Qi, Yao Mingfa, Yang Binbin, Qiu Lu, Reitz Rolf D. Development of an n-heptane/toluene/polyaromatic hydrocarbon mechanism and its application for combustion and soot prediction. Int J Engine Res 2013;14(5):434–51. https://doi.org/10.1177/1468087412471056.

[30] Pei Y, Mehl M, Liu W, Lu T, Pitz WJ, Som S. A Multicomponent Blend as a Diesel Fuel Surrogate for Compression Ignition Engine Applications. J Eng Gas Turbines Power 2015;137. https://doi.org/10.1115/1.4030416.

[32] Volgin SN, Belov IV, Likhterova NM, Ukhanov DA. Feasibility Study for Using Jet Fuel in Diesel Engines. Chem Technol Fuels Oils 2019;55(3):243–58. https://doi.org/10.1007/s10553-019-01027-3.

[33] Yu W, Zhao F, Yang W. Qualitative analysis of particulate matter emission from diesel engine fueled with Jet A-1 under multivariate combustion boundaries by principal component analysis. Appl Energy 2020;269:115068. https://doi.org/10.1016/j.apenergy.2020.115068.

[34] Cox AN. Allen's Astrophysical Quantities. 4th ed. Springer-Verlag New York; 2002. https://doi.org/10.1007/978-1-4612-1186-0.

[35] McBride BJ, Zehe MJ, Gordon S. NASA Glenn coefficients for calculating thermodynamic properties of individual species. 2002.

[36] Pal Rajinder. Chemical exergy of ideal and non-ideal gas mixtures and liquid solutions with applications. Int J Mech Eng Educ 2019;47(1):44–72. https://doi.org/10.1177/0306419017749581.

[37] Heywood JB. Inernal Combustion Engine Fundamentals, vol. 1. Singapore: McGraw-Hill; 1988.

[38] MANSOURI SH, HEYWOOD JB. Correlations for the Viscosity and Prandtl Number of Hydrocarbon-Air Combustion Products. Combust Sci Technol 1980;23(5–6):251–6. https://doi.org/10.1080/00102208008952416.

[39] Gordon S, McBride BJ. Computer Program for Calculation Complex Chemical Equilibrium Compositions and Applications I. Analysis. NASA Ref Publ 1311 1994:55.

[40] Gnielinski V. New Equations for Heat and Mass Transfer in Turbulent Pipe and Channel Flow. Int Chem Eng 1976;16:359–68.

[41] Bergman TL, Lavine AS, Incropera FP, Dewitt DP. Fundamentals of Heat and Mass Transfer. 7th ed. Ltd: John Wiley & Sons; 2011.

[42] Molki M, Sparrow EM. An Empirical Correlation for the Average Heat Transfer Coefficient in Circular Tubes. J Heat Transfer 1986;108:482–4. https://doi.org/10.1115/1.3246957.

[43] Szargut J. Chemical exergies of the elements. Appl Energy 1989;32:269–86. https://doi.org/10.1016/0306-2619(89)90016-0.

[44] Rivero R, Garfias M. Standard chemical exergy of elements updated. Energy 2006;31:3310–26. https://doi.org/10.1016/j.energy.2006.03.020.

[45] Holman JP. Experimental Methods for Engineers. 8th ed. McGraw-Hill; 2011.